



Associations between coronary/aortic ^{18}F -sodium fluoride uptake and pro-atherosclerosis factors in patients with multivessel coronary artery disease

Wanwan Wen, MD,^a Mingxin Gao, MD,^b Mingkai Yun, PhD,^a Jingjing Meng, MD,^a Ziwei Zhu, MD,^a Wenyuan Yu, MD,^b Marcus Hacker, MD,^c Yang Yu, MD, PhD,^b Xiaoli Zhang, MD, PhD,^a and Xiang Li, PhD^{a,c}

^a Department of Nuclear Medicine, Molecular Imaging Lab, Beijing Anzhen Hospital, Capital Medical University, Beijing, China

^b Department of Cardiac Surgery, Beijing Anzhen Hospital, Capital Medical University, Beijing, China

^c Division of Nuclear Medicine, Department of Biomedical Imaging and Image-guided Therapy, Vienna General Hospital, Medical University of Vienna, Vienna, Austria

Received Aug 3, 2021; accepted Mar 8, 2022

doi:10.1007/s12350-022-02958-x

Background. ^{18}F -NaF PET/CT is a novel approach to detect and quantify microcalcification in atherosclerosis. We aimed to explore the underlying systematic vascular osteogenesis in the coronary artery and aorta in patients with multivessel coronary artery disease (CAD).

Methods. Patients with multivessel CAD prospectively underwent ^{18}F -NaF PET/CT. The coronary microcalcification activity (CMA) and aortic microcalcification activity (AMA) were calculated based on both the volume and intensity of ^{18}F -NaF PET activity. Peri-coronary adipose tissue (PCAT) density was measured in adipose tissue surrounding the coronary arteries and the ^{18}F -NaF tissue-to-blood ratio (TBR) was measured in the coronary arteries.

Results. 100 patients with multivessel CAD were prospectively recruited. The CMA was significantly associated with the AMA ($r = 0.70$; $P < .001$). After multivariable adjustment, the CMA was associated with the AMA (Beta = 0.445 per SD increase; $P < .001$). The coronary TBR was also significantly associated with the PCAT density ($r = 0.56$; $P < .001$). The PCAT density was independently associated with the coronary TBR after adjusting confounding factors.

Conclusions. Coronary ^{18}F -NaF uptake was significantly associated with the PCAT density. There was a significant relationship between the coronary and the aortic ^{18}F -NaF uptake. It might indicate an underlying systematic vascular osteogenesis in patients with multivessel CAD. (J Nucl Cardiol 2022;29:3352–65.)

Key Words: Multivessel coronary artery disease • osteogenesis • inflammation • positron emission tomography • peri-coronary adipose tissue

Supplementary Information The online version contains supplementary material available at <https://doi.org/10.1007/s12350-022-02958-x>.

The authors of this article have provided a PowerPoint file, available for download at SpringerLink, which summarizes the contents of the paper and is free for re-use at meetings and presentations. Search for the article DOI on SpringerLink.com.

All editorial decisions for this article, including selection of reviewers and the final decision, were made by guest editor Rob deKemp, PhD. Wanwan Wen and Mingxin Gao have contributed equally to this work.

Funding: We thank the Key Medical Specialty Program of Sailing Plans organized by Beijing Municipal Administration of Hospitals (grant numbers: ZYLX202110) for supporting this research.

Reprint requests: Xiaoli Zhang, MD, PhD, Department of Nuclear Medicine, Molecular Imaging Lab, Beijing Anzhen Hospital, Capital Medical University, Beijing, China; xlzhang68@126.com

J Nucl Cardiol 2022;29:3352–65.

1071-3581/\$34.00

Copyright © 2022 The Author(s) under exclusive licence to American Society of Nuclear Cardiology

Abbreviations

¹⁸ F-NaF	¹⁸ F-sodium fluoride
CAD	Coronary artery disease
CT	Computed tomography
LAD	Left anterior descending
LCX	Left circumflex
PCAT	Peri-coronary adipose tissue
PET	Positron emission tomography
RCA	Right coronary artery
SUV	Standardized uptake value
TBR	Tissue-to-background ratio

See related editorial, pp. 3366–3368

INTRODUCTION

Coronary atherosclerotic plaque rupture is the principal cause of acute coronary syndrome and a significant cause of sudden cardiac death and its prevention is crucial.^{1,2} Plaque rupture events are challenging to predict because the most culprit lesions are non-flow limiting and often overlooked by traditional functional investigations. Novel imaging techniques now have a potential to identify the pathological structures and processes in association with plaque rupture. During atherosclerosis progression, macrophage-derived cytokines induce osteogenic differentiation and vascular cell mineralization, suggesting that pro-inflammatory molecules could promote atherosclerotic osteogenesis by regulating the differentiation of calcified vascular cells.³ Active microcalcification in the atherosclerotic plaque is considered as a marker of cell death and inflammation and carries an increased risk of plaque rupture and associated complications.⁴

Multivessel coronary artery disease (CAD) is a common manifestation of advanced coronary atherosclerosis. In complex cardiovascular disorders, the relevance of systemic causes of atherosclerosis development and progression is widely recognized. Patients who have multivessel CAD may have concomitant systemic atherosclerosis in multiple arterial beds, given that they share the same risk factors and genetic predispositions.⁵ Nonetheless, there is no evidence demonstrating the underlying systematic vascular osteogenesis in patients with multivessel CAD. The positron emission tomography (PET) tracer ¹⁸F-sodium fluoride (¹⁸F-NaF) is a marker of developing microcalcification and osteogenic activity across multiple different cardiovascular disease states.^{6,7} ¹⁸F-NaF PET/computed tomography (CT), as a non-invasive imaging technique, could be a novel approach to visualize and quantify biochemical

osteogenic activity in the systematic vasculature with high sensitivity.^{8–10}

Peri-coronary adipose tissue (PCAT), a source of pro-atherogenic mediators, is closely adjacent to the coronary artery tree has been demonstrated that increased density of PCAT plays an essential role in the development of coronary atherosclerosis through bidirectional communication with the vessel wall at a cellular level.^{11,12} Recent studies have demonstrated the PCAT is associated with focal coronary ¹⁸F-NaF PET uptake in stable CAD patients.^{13,14} Nevertheless, the relationship between PCAT density and ¹⁸F-NaF PET uptake in multivessel CAD patients has not been characterized. In addition, new-onset or rapid coronary calcification progression is associated with an enhanced risk for future CAD events and cardiovascular risk prediction can be enhanced by examining the coronary artery calcium burden.

In the present study, we firstly aimed to evaluate the underlying systematic vascular osteogenesis in cardiovascular by analyzing the association between the coronary and the aortic ¹⁸F-NaF uptake in patients with multivessel CAD, and further to evaluate the associations between coronary artery osteogenic activity and conventional pro-atherosclerosis factors, including PCAT density, coronary artery calcium burden, CAD risk factors, and serum biomarkers.

METHODS

Patient population

This observational cross-sectional study was a monocentric pilot study as a prospective trial registered with the Chinese Clinical Trial Registry (ChiCTR1900022527). It was aimed to investigate the performance of ¹⁸F-NaF PET/CT in the characterization of coronary plaque in patients with multivessel CAD. A total of 457 consecutive patients with CAD were prospectively included in Beijing Anzhen Hospital between February 2018 and April 2021. Patients with multivessel CAD confirmed by coronary angiographically were included, which defined as presenting at least 2 of 3 epicardial vessels with a stenosis $\geq 70\%$ or left the main stenosis $\geq 50\%$. Cardiac ¹⁸F-NaF PET/CT scan were performed within 14 days of the coronary angiography. Patients were excluded if (1) a recent myocardial infarction (< 4 weeks), (2) history of malignancy, acute or chronic inflammatory, and autoimmune disease (3) history of cardiovascular surgery. Finally, a total of 100 multivessel CAD patients were recruited in our current study. The study flow chart is shown in Figure 1. The project was approved by the Medicine Ethics Committee

of Beijing Anzhen Hospital (2018055X) and adhered to the principles laid out in the Declaration of Helsinki.

Assessment of SYNTAX score

Patients were scored for anatomic complexity by the SYNTAX scores using an online calculator system (<http://www.syntaxscore.com/calculator/start.htm>). The SYNTAX scoring was a comprehensive angiographic assessment of the coronary vasculature, with 0 as the lowest score and the higher scores [no upper limit] indicating the more complex coronary anatomy. All evaluations were conducted by two cardiac surgeons (GM and YW), blinded to the patients' data.

Cardiac ^{18}F -NaF PET/CT and image analysis

All patients were administered a target dose of ^{18}F -NaF (3.7 MBq/kg) intravenously and subsequently rested in a quiet environment for a 120-minute uptake period,¹⁵ an electrocardiogram-gated cardiac ^{18}F -NaF PET/CT imaging (Biograph mCT, Siemens Medical Systems, Erlangen, Germany) was performed. Then, a low-dose attenuation correction CT scan (120 kV, 50 mAs) was acquired. The PET data were reconstructed using a point spread function + time of flight algorithm (time of flight + TrueX, Siemens Ultra-HD), with 5 iterations and 21 subsets. Due to the small size of the vulnerable plaques, an in-plane pixel size of 2 mm with

a corresponding reconstructed image matrix size of 400×400 was used to achieve a high spatial resolution.

To evaluate the coronary ^{18}F -NaF uptake, semi-quantitative analysis was performed by obtaining the maximum standardized uptake value (SUV) (a validated measure of tissue radiotracer uptake) by manually placing the regions of interest (delimiting three-dimensional regions) in the proximal of left anterior descending (LAD), left circumflex (LCX), and right coronary artery (RCA). The tissue-to-background ratio (TBR) in the LAD (TBR_{LAD}), LCX (TBR_{LCX}), and RCA (TBR_{RCA}) were then calculated by correction for background blood-pool activity using the right atrium (mean SUV using cylindrical volumes of interest [radius: 10 mm; thickness: 5 mm] at the level of the RCA ostium), respectively. The TBR in the coronary artery was calculated as the average TBR value from three main coronary arteries (LAD, LCX, and RCA) in each patient.

Coronary microcalcification activity, which represents the overall disease activity in the main coronary arteries (LAD, LCX, and RCA) and based upon both the volume and intensity of ^{18}F -NaF PET activity within it, was defined as the integrated activity in SUV units exceeding the background blood-pool $\text{SUV}_{\text{mean}} + 2$ standard deviations (left atrium activity).¹⁶ These encompass all the main epicardial coronary vessels and their immediate surroundings (4-mm radius), facilitating per-vessel and per-patient uptake quantification. Coronary microcalcification activity was calculated by a

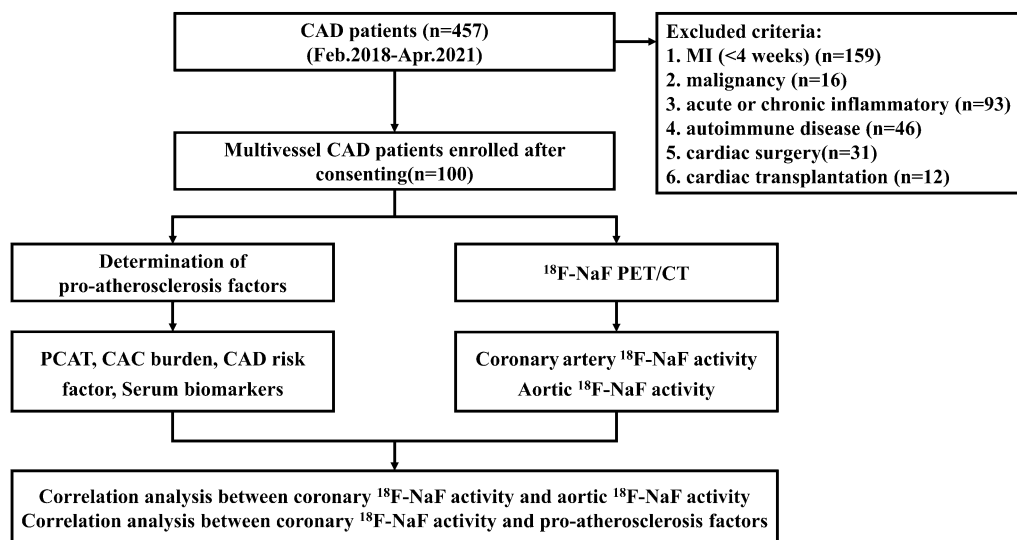


Figure 1. Study design flowchart. Flowchart of the included and excluded criteria of the present study. ^{18}F -NaF, ^{18}F -sodium fluoride; CAC, Coronary artery calcium score; CAD, coronary artery disease; MI, myocardial infarction; PCAT, peri-coronary adipose tissue; PET/CT, positron emission tomography/computed tomography.

formula for normalizing measurement: Coronary microcalcification activity = $([\text{LAD cumulative SUV} + \text{LCX cumulative SUV} + \text{RCA cumulative SUV}] / [\text{LAD volume} + \text{LCX volume} + \text{RCA volume}]) / ([\text{right atrial cumulative SUV} + \text{left atrial cumulative SUV}] / [\text{right atrial volume} + \text{left atrial volume}])$.

The aortic (ascending aorta, aortic arch) ¹⁸F-NaF uptake was determined within volumes of interest created around the aorta using a centerline function in a multiplanar reconstruction. The ascending aortic volume of interest started at the sinotubular junction and finished immediately proximal to the junction with the brachiocephalic artery. The aortic arch volume of interest started from the junction with the brachiocephalic artery and finished immediately distal to the junction with the left subclavian artery. Aortic microcalcification activity was calculated by dividing aortic intensity per cm³ $([\text{ascending cumulative SUV} + \text{arch cumulative SUV}] / [\text{ascending volume} + \text{arch volume}])$ by background intensity per cm³ $([\text{right atrial cumulative SUV} + \text{left atrial cumulative SUV}] / [\text{right atrial volume} + \text{left atrial volume}])$ as a unitless number.⁸

Analysis of coronary artery calcium burden and PCAT on CT

Cardiac CT scans were conducted with electrocardiography-gated cardiac CT using a 128-slice multi-detector computed tomography scanner (Biograph mCT, Siemens Healthcare, Erlangen, Germany) (following cardiac PET/CT scans immediately). The scan parameters were: 128 x 0.6 mm collimation; tube voltage, 120 kV; gantry rotation time, 330ms; and tube current, 770–850 mAs. Coronary calcium was quantified on both a per-patient and per-segment level by an experienced observer (WW) using volume analysis software (Cascoring Siemens Healthcare, mCT). The coronary artery calcium score was derived using the Agatston method. To quantify the PCAT density, a CT attenuation threshold of -190 to -30 Hounsfield Units¹⁷ was used to isolate adipose tissue by Mimics Medical software (version 21.0; Materialise, Leuven, Belgium),¹⁸ and the PCAT density was defined as the mean attenuation within such contamination-free volumes of interest and was measured in adipose tissue surrounding the proximal of LAD, LCX and RCA, where adjacent to the regions of interest of ¹⁸F-NaF uptake measurement. For each coronary artery, five regions of interest (each regions of interest area = 3 mm²) were manually placed on the region of distance the outer coronary artery wall, width equal to the vessel diameter.¹⁹ The PCAT density of the LAD (PCAT_{LAD}), LCX (PCAT_{LCX}) and RCA (PCAT_{RCA}) was calculated by the average PCAT value from the value of five regions of interest in LAD, LCX,

and RCA, respectively. The PCAT density in each patient was calculated as the average PCAT value from three main coronary arteries (LAD, LCX, and RCA). PCAT density measurement by cardiac CT was performed by two experienced nuclear cardiologists (MJ and WW), who were blinded to the quantitative analysis data as well as ¹⁸F-NaF PET/CT image analysis.

Statistical analysis

All statistical analyses were performed using SPSS software (version 25, SPSS, Inc., Chicago, IL). Continuous variables were tested for normality using Shapiro–Wilk test and were presented as mean ± standard deviation or median (interquartile range) dependent on the distribution. Data were compared by using two-sample *t*-test or Mann–Whitney *U* tests. Categorical variables were summarized using frequencies and percentages and were compared by using a Chi-squared test (with a Yates correction or a Fisher exact test for smaller sample sizes). Patients were divided dichotomously by the median coronary microcalcification activity value into two groups (coronary microcalcification activity < 1.42, *n* = 50; coronary microcalcification activity ≥ 1.42, *n* = 50). Patients were also divided dichotomously by the median coronary TBR value into group 1 (coronary TBR ≥ 2.49, *n* = 50) and group 2 (coronary TBR < 2.49, *n* = 50). Spearman’s correlation analysis and multiple linear regression analysis were used to assess the correlations between the coronary ¹⁸F-NaF uptake with the aortic ¹⁸F-NaF uptake, PCAT density, coronary artery calcium burden, CAD risk factors, and serum biomarkers, respectively. To quantify the inter- and intraobserver reproducibility of the coronary ¹⁸F-NaF uptake, the aortic ¹⁸F-NaF uptake, and PCAT density measurements, the intraclass correlation coefficients were calculated and Bland-Altman analysis was undertaken. A 2-sided *P*-value < .05 was regarded as significant.

RESULTS

Baseline clinical characteristics of the study population

Baseline characteristics of study population are listed in Table 1. A total of 100 multivessel CAD patients were enrolled (age 64.00 [57.00–67.75] years; 76 men; NYHA class III/IV: 63%; hyperlipidemia: 58%; hypertension: 71%), widespread utilization of secondary preventative therapies aspirin: 82%; statins: 87%; Beta-blocker: 75%. The PCAT density and coronary artery calcium score were -79.50 (-86.62 to -73.58) and 808.00 (213.30–1646.30), respectively. Serum

Table 1. Baseline clinical characteristics of the study population

	n = 100
Baseline characteristics	
Age, years	64.00 (57.00-67.75)
Men, n (%)	76 (76.00)
Body-mass index, kg/m ²	24.88 (23.08-27.33)
LVEF, %	59.00 (48.50-65.00)
Systolic blood pressure, mmHg	129.00 (120.00-141.75)
Diastolic blood pressure, mmHg	73.00 (67.00-79.00)
NYHA class III/IV, n (%)	63 (63.00)
Diabetes, n (%)	38 (38.00)
Hyperlipidemia, n (%)	58 (58.00)
Hypertension, n (%)	71 (71.00)
Smoker, n (%)	57 (57.00)
Family history of CAD, n (%)	35 (35.00)
Serum biomarkers	
High-density lipoprotein, mmol/L	0.97 (0.85-1.13)
Low-density lipoprotein, mmol/L	2.17 (1.81-2.86)
High-sensitivity C-reactive protein, mg/L	2.56 (0.86-15.15)
Interleukin-6, pg/mL	6.40 (4.20-8.40)
Tumor necrosis factor alpha, pg/mL	9.27 (7.50-13.30)
Creatinine clearance rate, mL/min	87.00 (70.00-101.00)
Troponin I, ng/mL	0.01 (0.00-0.05)
Medications, n (%)	
Aspirin	82 (82.00)
Statins	87 (87.00)
ACEIs/ARBs	32 (32.00)
Beta-blocker	75 (75.00)
SYNTAX score	55.00 (44.25-70.00)
Coronary artery calcium score	808.00 (213.30-1646.30)
PCAT	
PCAT _{LAD}	- 79.50 (- 86.62 to - 73.58)
PCAT _{LCX}	- 81.81 (- 90.72 to - 74.39)
PCAT _{RCA}	- 78.20 (- 86.85 to - 70.60)
PET/CT	
Coronary microcalcification activity	1.42 (1.21-1.86)
Aortic microcalcification activity	1.28 (1.11-1.45)

Data are presented as median (25th to 75th percentile) or n (%).

ACEI, angiotensin-converting enzyme inhibitor; ARB, angiotensin receptor blocker; CAD, coronary artery disease; CT, computed tomography; LVEF, left ventricular ejection function; NYHA, New York Heart Association; LAD, left anterior descending; LCX, left circumflex; PCAT, peri-coronary adipose tissue; PET, positron emission tomography; RCA, right coronary artery

biomarkers were presented in the following: high-density lipoprotein: 0.97 (0.85-1.13) mmol/L; low-density lipoprotein: 2.17 (1.81-2.86) mmol/L; high-sensitivity C-reactive protein: 2.56 (0.86-15.15) mg/L; interleukin-6: 6.40 (4.20-8.40) pg/mL; tumor necrosis factor alpha: 9.27 (7.50-13.30) pg/mL; creatinine clearance rate: 87.00 (70.00-101.00) mL/min; and troponin I: 0.01 (0.00-0.05) ng/mL.

Reproducibility of measurements

Excellent agreement was observed in the interobserver variabilities of coronary microcalcification activity, aortic microcalcification activity, coronary TBR, and PCAT. There was also a substantial agreement between the intraobserver variabilities for coronary microcalcification activity, aortic microcalcification activity, coronary TBR, and PCAT (Additional file:

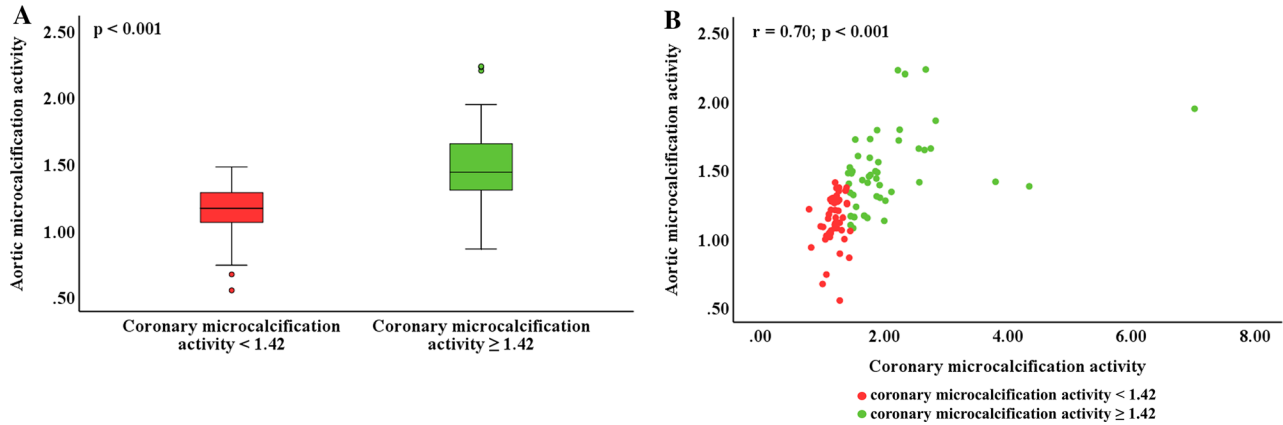


Figure 2. Correlation between the CMA and the AMA. Patient with higher CMA (≥ 1.42) had a higher AMA [1.44 (1.29-1.65) vs 1.16 (1.06-1.28); $P < .001$] than those with lower CMA (< 1.42) (A). There was a moderate correlation between the CMA and the AMA ($r = 0.70$; $P < .001$) (B). CMA, coronary microcalcification activity; AMA, aortic microcalcification activity.

Table S1). In the Bland-Altman analysis, the interobserver variabilities were 0.10 ± 0.88 for coronary microcalcification activity, -0.05 ± 0.28 for aortic microcalcification activity, -0.02 ± 0.99 for coronary TBR, and 0.63 ± 4.68 for PCAT (mean ± 1.96 SD). Bland-Altman analyses showed a good intraobserver reproducibility with no fixed biases for the quantification of coronary microcalcification activity (0.03 ± 0.27), aortic microcalcification activity (0.03 ± 0.20), coronary TBR (-0.01 ± 0.20), and PCAT (-0.20 ± 5.09) (mean ± 1.96 SD) (Additional file: Figure S1, Figure S2, Figure S3, and Figure S4).

Correlations between the coronary ¹⁸F-NaF Uptake and the Aortic ¹⁸F-NaF uptake

Compared with patients with lower coronary microcalcification activity (< 1.42 , $n = 50$), the aortic microcalcification activity was significantly increased [1.44 [1.29-1.65] vs 1.16 [1.06-1.28]; $P < .001$] in patients with higher coronary microcalcification activity (≥ 1.42 , $n = 50$) (Figure 2A). The aortic microcalcification activity was also significantly correlated with the coronary microcalcification activity ($r = 0.70$, $P < .001$) (Figure 2B). Moreover, after adjustment confounding factors (age, gender, body-mass index), increased coronary microcalcification activity was independently associated with the aortic microcalcification activity (Beta: 0.445 per SD increase; 95% confidence interval: 0.303 to 0.587; $P < 0.001$) by multiple linear regression analysis. After adjustment for SYNTAX score and coronary artery calcium score, higher coronary microcalcification activity was also independently associated with the aortic microcalcification activity (Beta: 0.515

per SD increase; 95% confidence interval: 0.311 to 0.719; $P < .001$). Concordant associations were found after adjustment for combined cardiac risk factors and serum biomarkers (Table 2). Representative images in patients with significantly elevated coronary ¹⁸F-NaF uptake and aortic ¹⁸F-NaF uptake are illustrated in Figure 3.

Correlation between the coronary ¹⁸F-NaF uptake with the PCAT density

As shown in Table 3, the coronary TBR was significantly correlated with the PCAT density ($r = 0.56$, $P < .001$). There were significant correlations between the TBR value and the corresponding PCAT density in LAD, LCX, and RCA territories ($r = 0.47$, $P < .001$; $r = 0.36$, $P < .001$; $r = 0.41$, $P < .001$; respectively) (Figure 4). Per patient, we found that the PCAT density was independently associated with the coronary TBR (Beta: 0.448 per SD increase; 95% confidence interval: 0.286-0.610; $P < .001$) by multiple linear regression analysis (age, sex, body-mass index as covariates). After adjustment for SYNTAX score and coronary artery calcium score, the PCAT density was also independently associated with the coronary TBR (Beta: 0.416 per SD increase; 95% confidence interval: 0.222-0.610; $P < .001$). Significant associations were found after adjustment for combined cardiac risk factors and serum biomarkers (Table 4). Representative images are illustrated for PCAT and TBR in Figure 5.

Table 2. Univariate and multivariate linear regression analysis for the coronary microcalcification activity

Aortic microcalcification activity	Coronary microcalcification activity	
	Beta (95% confidence interval)	P
Univariate		
Per unit change	1.506 (1.043-1.969)	< .001
Per SD change	0.449 (0.311-0.587)	< .001
Covariate: age, sex, body-mass index		
Per unit change	1.494 (1.018-1.969)	< .001
Per SD change	0.445 (0.303-0.587)	< .001
Covariate: combined cardiac risk factors ^a		
Per unit change	1.430 (0.939-1.922)	< .001
Per SD change	0.426 (0.280-0.572)	< .001
Covariate: serum biomarkers ^b		
Per unit change	0.972 (0.497-1.447)	< .001
Per SD change	0.290 (0.148-0.431)	< .001
Covariate: SYNTAX score, coronary artery calcium score		
Per unit change	1.728 (1.043-2.413)	< .001
Per SD change	0.515 (0.311-0.719)	< .001

Beta, Unstandardized regression coefficients; CAD, coronary artery disease

^aAdjusted for diabetes, hyperlipidemia, hypertension, smoker, family history of CAD

^bAdjusted for high-density lipoprotein, low-density lipoprotein, high-sensitivity C-reactive protein, interleukin-6, tumor necrosis factor alpha, creatinine clearance rate, troponin I

Correlation between CAD risk factors, serum biomarkers with coronary ¹⁸F-NaF uptake

There was a significant association between the coronary TBR and the coronary artery calcium score ($r = 0.45$, $P < .001$) (Table 3). The coronary artery calcium score was significantly higher in group 1 compared with that in group 2 ($P < .001$) (Supplemental file: Table S2).

Age in all individuals was significantly correlated with the coronary TBR ($r = 0.24$, $P = .019$) (Table 3). Patients in group 1 were relatively older ($P = .002$) (Supplemental file: Table S2).

Serum troponin I level in all individuals was correlated with the coronary TBR ($r = 0.22$, $P = .039$) (Table 3). There were no significant correlations between traditional CAD risk factors (e.g., diabetes, hyperlipidemia, hypertension, smoker, family history of CAD, high-density lipoprotein, low-density lipoprotein, high-sensitivity C-reactive protein, interleukin-6, tumor necrosis factor alpha, and creatinine clearance rate) with the coronary TBR (Table 3).

DISCUSSION

In the present study, we found that the coronary ¹⁸F-NaF uptake was positively and independently correlated with the aortic ¹⁸F-NaF uptake in patients with multivessel CAD. Furthermore, there was also a strong correlation between the coronary ¹⁸F-NaF uptake and the PCAT density as well as the coronary artery calcium score. Our results suggested that the presence of systematic vascular osteogenesis activation in the coronary artery and the aorta in multivessel CAD patients. In addition, this study highlighted that ¹⁸F-NaF PET/CT imaging can provide important supplemental information for identifying patients with multivessel CAD who are at excess vascular risk.

Atherosclerosis is a fundamental pathogenic process in many diseases, including cerebrovascular and cardiovascular diseases, aortic aneurysm/dissection, and arteriosclerosis obliterans. Plaque is known to be the major characteristics of atherosclerosis and various pathophysiologic processes are involved in the formation and progression of atherosclerotic plaque, including inflammation, apoptosis, and mineralization.²⁰ Microcalcification, which represents a specific phase in the evolution of an atheroma, is a key feature of atherosclerotic plaque rupture, that is embedded in the fibrous cap

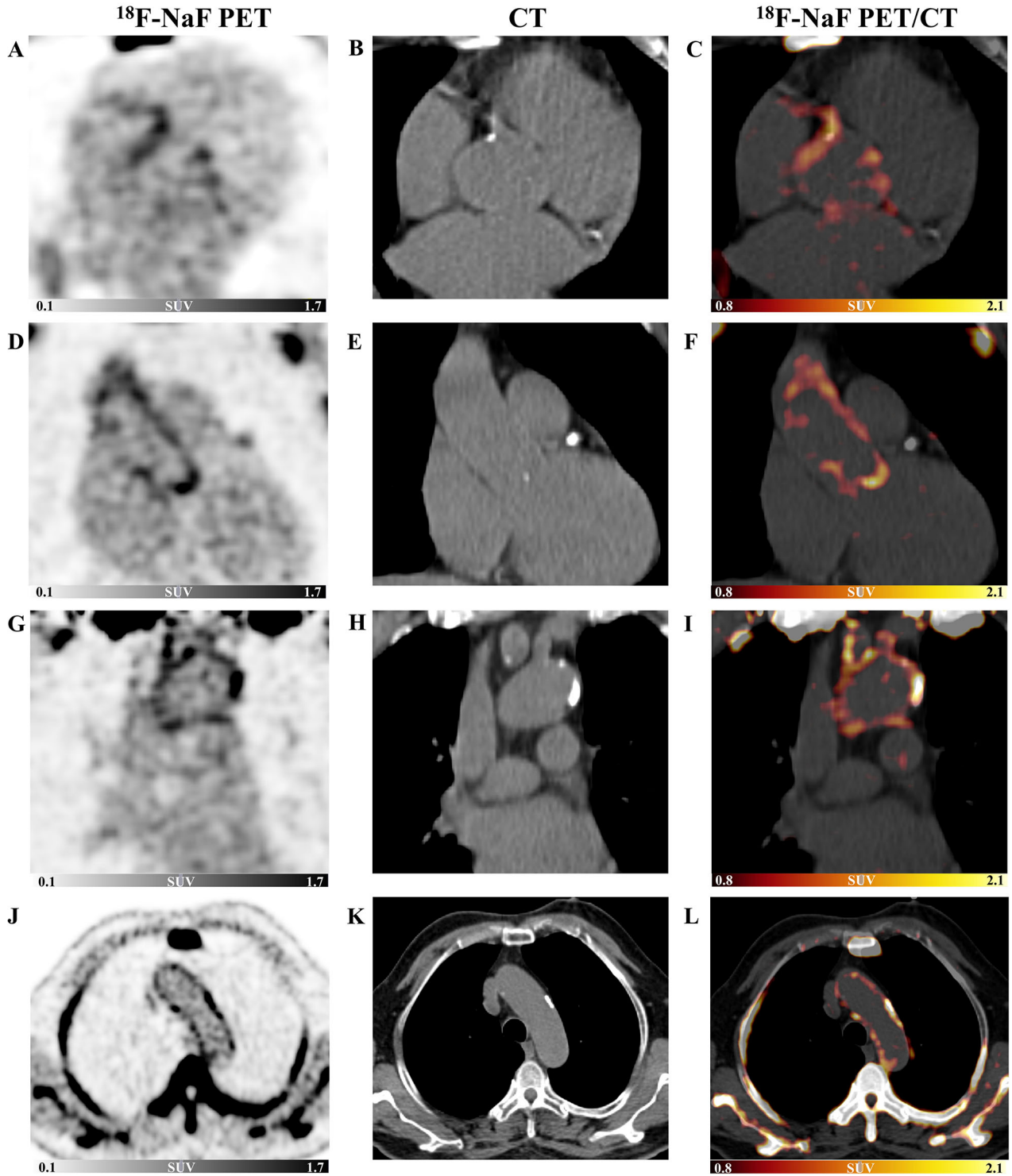


Figure 3. Representative case showing the ^{18}F -NaF PET/CT in patients with significantly elevated coronary and aortic ^{18}F -NaF uptake. Patient (male; 72 years) suffered multivessel lesions presenting an intense focal ^{18}F -NaF uptake in LCX and RCA (A-C). Coronal view of the thorax showing increased ^{18}F -NaF uptake in the ascending aorta (D-F) and aortic arch (G-I). Short-axis view of the thorax showing increased ^{18}F -NaF uptake in the aortic arch (J-L). ^{18}F -NaF, ^{18}F -sodium fluoride; LCX, left circumflex; PET/CT, positron emission tomography/computed tomography; RCA, right coronary artery.

Table 3. Correlation between the coronary TBR and clinical variables

	Coronary TBR	
	<i>r</i>	<i>P</i>
Baseline characteristics		
Age, years	0.24	.019
Men, n (%)	0.15	.16
BMI, kg/m ²	0.03	.79
LVEF, %	− 0.13	.24
Systolic blood pressure, mmHg	0.21	.048
Diastolic blood pressure, mmHg	0.06	.59
NYHA class III/IV, n (%)	0.06	.58
Diabetes, n (%)	0.07	.50
Hyperlipidemia, n (%)	0.07	.52
Hypertension, n (%)	0.15	.16
Smoker, n (%)	0.12	.24
Family history of CAD, n (%)	0.07	.51
Serum biomarkers		
High-density lipoprotein, mmol/L	0.06	.56
Low-density lipoprotein, mmol/L	− 0.05	.61
High-sensitivity C-reactive protein, mg/L	0.04	.72
Interleukin-6, pg/mL	0.19	.11
Tumor necrosis factor alpha, pg/mL	− 0.02	.80
Creatinine clearance rate, mL/min	0.11	.29
Troponin I, ng/mL	0.22	.039
Medications, n (%)		
Aspirin	0.02	.85
Statins	0.03	.77
ACEIs/ARBs	0.11	.31
Beta-blocker	0.02	.85
SYNTAX score	0.07	.56
Coronary artery calcium score	0.45	< .001
PCAT	0.56	< .001

ACEI, angiotensin-converting enzyme inhibitor; ARB, angiotensin receptor blocker; BMI, body-mass index; CAD, coronary artery disease; CT, computed tomography; LVEF, left ventricular ejection function; NYHA, New York Heart Association; PCAT, pericoronary adipose tissue; TBR, tissue-to-background ratio

of atherosclerotic plaques and, then lead to considerable stress accumulation in the fibrous cap and destabilize the structural integrity of the fibrous cap.²¹

It was not surprising that patients with multivessel CAD frequently had atherosclerosis in other arteries, due to they shared the same pathophysiological mechanisms.²² Several studies reported significant associations of coronary with extra-cardiac atherosclerotic disease (such as the carotid, renal or lower limb arteries).^{23,24} However, to our knowledge, none of these studies thoroughly performed a systemic vascular osteogenesis examinations on coronary and aorta in patients with complex CAD. In addition, prior studies did not use

systemic vascular imaging modalities to evaluate the systemic atherosclerosis. ¹⁸F-NaF is an well-established PET bone tracer that binds to hydroxyapatite, a crystalline structure that is a key component of microcalcification.²⁵ ¹⁸F-NaF PET/CT imaging, as a promising non-invasive imaging tool, can be used to identify the systematic vascular osteogenesis in multiple arteries by binding to hydroxyapatite.

Given the same cardiovascular risk factors and genetic predispositions, the prevalence and development of aortic plaque are closely related to coronary artery atherosclerosis, which was consistent with an underlying systemic vascular atherosclerotic process. McGill et al

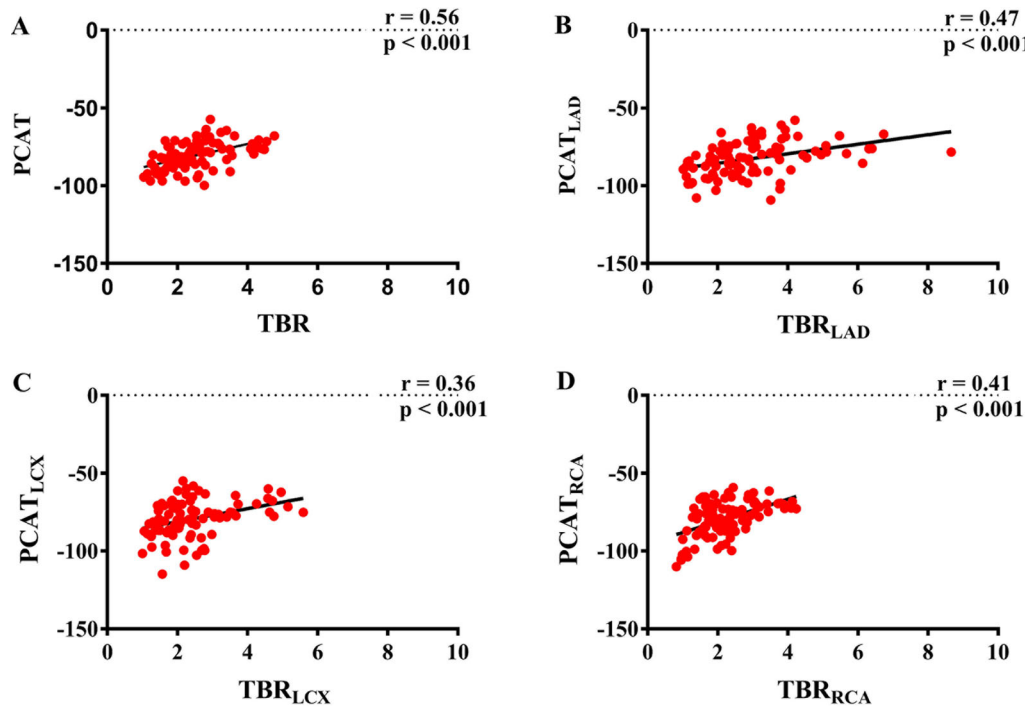


Figure 4. Correlations between the PCAT and the coronary TBR. Scatterplots of PCAT vs TBR (A), PCAT_{LAD} vs TBR_{LAD} (B), PCAT_{LCX} vs TBR_{LCX} (C), PCAT_{RCA} vs TBR_{RCA} (D). *r*, spearman correlation coefficients; *LAD*, left anterior descending; *LCX*, left circumflex; *PCAT*, peri-coronary adipose tissue; *RCA*, right coronary artery; *TBR*, tissue-to-background ratio.

found a concordant pattern of raised fatty streaks in the abdominal aorta and the RCA.²⁶ In addition, a recent cross-sectional observation study demonstrated that asymptomatic and spontaneous aortic plaque rupture was detected in 80% of patients with suspected or diagnosed CAD.²⁷ In our study, we found that the coronary ^{18}F -NaF uptake was independently correlated with the aortic ^{18}F -NaF uptake in patients who had advanced multivessel CAD and concomitant cardiovascular risk factors (hyperlipidemia and hypertension). Our study revealed an interactive connection of systematic vascular osteogenesis within the different vascular beds. It might demonstrate a concomitant microcalcification activation in symptomatic CAD patients. Thus, simultaneous screening the systemic osteogenesis in the multiple vasculatures may clarify the precise pathophysiological conditions and mechanisms underlying multivascular disease.

PCAT is an ectopic thoracic fat tissue located between the visceral layer of the pericardium and the myocardium, surrounding the coronary artery tree.^{11,12} A large body of evidence, including experimental and clinical studies, has demonstrated that PCAT is a recognized source of pro-inflammatory mediators in high-risk cardiac patients, which can directly modulate

the coronary artery through the mechanism of paracrine and autocrine.^{28,29} Moreover, several studies have indicated that the relationship of adipose tissue and the vascular wall is a complex interaction, PCAT releases a wide range of bioactive molecules that exert endocrine and paracrine effects on the vascular lipid metabolism and vascular inflammation.^{30,31} ^{18}F -NaF PET/CT has emerged as a non-invasive quantitative imaging modality and is able to measure the microcalcification activity in the vasculature.^{4,32} In this study, we conducted an observational cross-sectional study with a relatively larger number of patients with multivessel CAD and found a significant correlation between the coronary ^{18}F -NaF activity and the PCAT density, which was concordant with findings by previous studies,^{13,14} who demonstrated an association of increased PCAT CT attenuation with higher ^{18}F -NaF PET activity in forty patients with high-risk plaques. In contrast to previous studies, we performed delay PET scans (120-minute), providing a minimal blood-pool activity, a higher TBR, and a higher SUVmax, and thus, improving the detection of ^{18}F -NaF uptake in coronary artery plaques and aorta plaques.¹⁵ In addition, in comparison with prior studies, our research enrolled more advanced CAD patients who had multivessel lesions. Although the severity of

Table 4. Univariate and multivariate linear regression analysis for coronary TBR

PCAT	Coronary TBR	
	Beta (95% confidence interval)	P
Univariate		
Per 10 HU change	0.512 (0.331–0.693)	< .001
Per SD change	0.465 (0.300–0.629)	< .001
Covariate: age, sex, body-mass index		
Per 10 HU change	0.494 (0.315–0.672)	< .001
Per SD change	0.448 (0.286–0.610)	< .001
Covariate: combined cardiac risk factors ^a		
Per 10 HU change	0.508 (0.320–0.696)	< .001
Per SD change	0.461 (0.291–0.632)	< .001
Covariate: serum biomarkers ^b		
Per 10 HU change	0.529 (0.300–0.758)	< .001
Per SD change	0.480 (0.272–0.688)	< .001
Covariate: SYNTAX score, coronary artery calcium score		
Per 10 HU change	0.458 (0.245–0.672)	< .001
Per SD change	0.416 (0.222–0.610)	< .001

^aAdjusted for diabetes, hyperlipidemia, hypertension, smoker, family history of CAD

^bAdjusted for high-density lipoprotein, low-density lipoprotein, high-sensitivity C-reactive protein, interleukin-6, tumor necrosis factor alpha, creatinine clearance rate, troponin I
Beta, Unstandardized regression coefficients; *CAD*, coronary artery disease; *PCAT*, peri-coronary adipose tissue; *TBR*, tissue-to-background ratio

systemic atherosclerotic pathology may have a significant effect on inflammation and osteogenesis, our study found that the coronary TBR was independently associated with the corresponding PCAT density, which indicating there was a significant correlation between osteogenesis and inflammation in atherosclerosis, regardless of CAD severity.

Pioneering studies demonstrated that the coronary ¹⁸F-NaF uptake was significantly correlated with the coronary artery calcium score and the progression of coronary calcification.^{33,34} Increased coronary ¹⁸F-NaF uptake was significantly associated with more rapid progression of coronary calcification at one year in patients with clinically stable multivessel CAD.³³ Intriguingly, we also found that coronary ¹⁸F-NaF uptake was significantly correlated with the calcium burden in the coronary artery assessed by cardiac non-contrast CT. These results may indicate that the underlying correlation between the accumulation of ¹⁸F-NaF and the corresponding incremental change during the calcified plaque progression.

Cardiac troponin I was used to detecting myocardial necrosis as a preferred biomarker in the diagnosis of myocardial infarction.³⁵ Joshi et al reported an association between increased coronary ¹⁸F-NaF uptake and higher plasma high-sensitivity cardiac troponin I

concentration in patients with stable CAD.³⁶ Our study also observed that serum troponin I level was associated with coronary ¹⁸F-NaF uptake in patients with multivessel CAD. In fact, silent plaque rupture and subclinical plaque thrombus formation are frequent incidental post-mortem findings in patients with multivessel CAD. These results suggest that coronary ¹⁸F-NaF PEC/CT imaging might provide complementary information over traditional standard risk factors.

Limitations

This study had several limitations. First, this was a single-center study in patients with multivessel CAD, and bias selection was possible; however, adjustments were made for the confounding effects of risk factors for the association between the PCAT density and the coronary ¹⁸F-NaF activity. Second, partial volume effects and cardiac motion could have affected the PET quantification in the coronary artery lesions. Third, CT angiography was not performed in this study cohort. Finally, the patient outcome assessment is lacking in the current study, which is warranted for the future investigation.

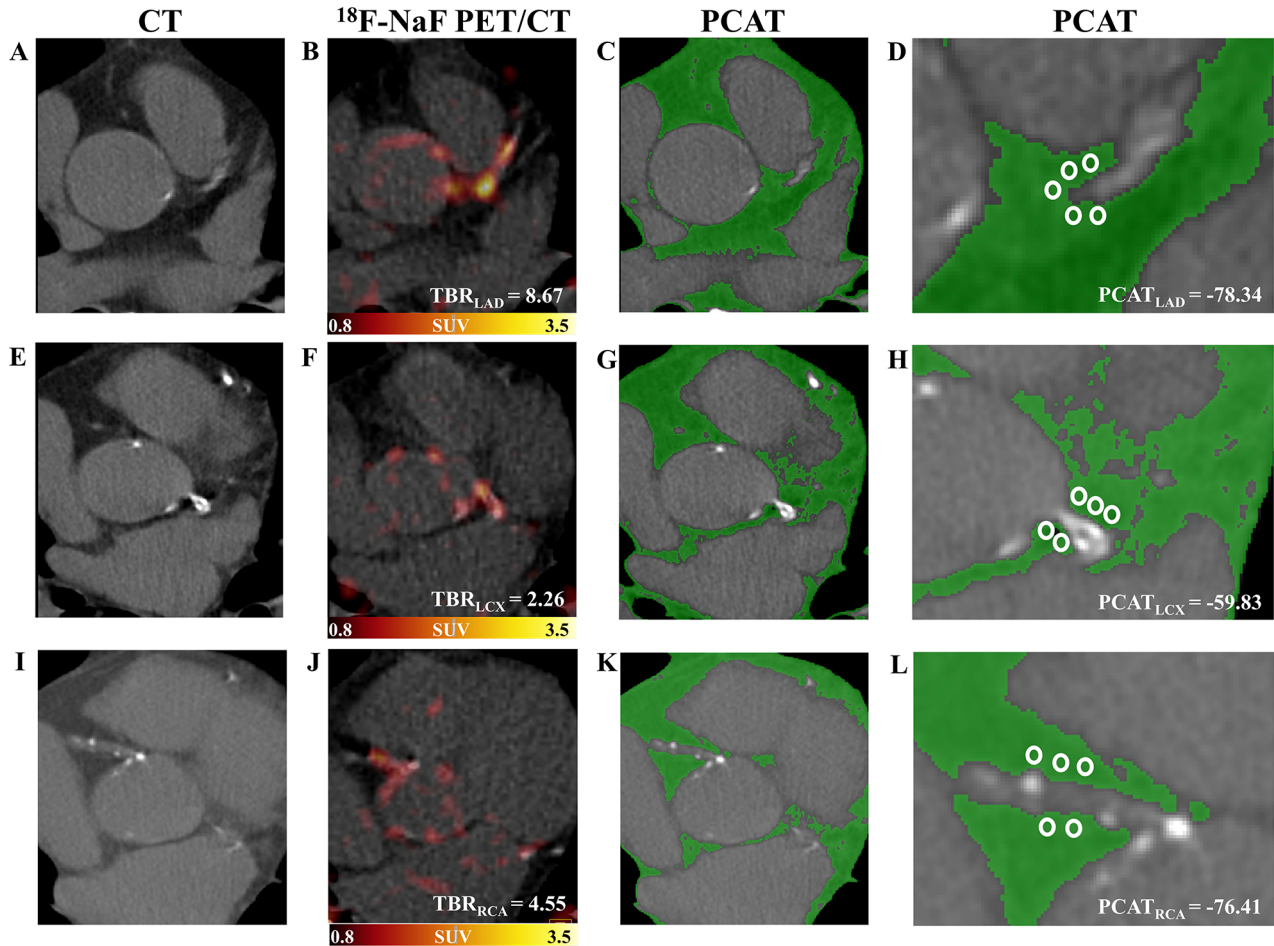


Figure 5. Representative case showing the relationship between the coronary TBR with the PCAT in a patient with prominent ^{18}F -NaF uptake. Patient (male; 64 years) suffered multivessel lesions presenting intense focal ^{18}F -NaF uptake in LAD (A, B), LCX (E, F), RCA (I, J). Epicardial adipose area (green) for placing five regions of interest (3 mm^2) and measuring PCAT density surrounding the LAD (C, D), LCX (G, H), RCA (K, L). ^{18}F -NaF, ^{18}F -sodium fluoride; LAD, left anterior descending; LCX, left circumflex; PCAT, peri-coronary adipose tissue; RCA, right coronary artery; TBR, tissue-to-background ratio.

NEW KNOWLEDGE GAINED

This study showed that the coronary ^{18}F -NaF uptake was related to the aortic ^{18}F -NaF uptake and was also correlated with the pro-atherosclerosis factors (including PCAT density, coronary artery calcium score). ^{18}F -NaF PET/CT, a simple and repeatable method for quantifying microcalcification activity in the coronary artery and the aorta, can contribute to provide complementary information for identifying systematic vascular osteogenesis in patient with multivessel CAD. There is a possible indication that the ^{18}F -NaF PET/CT may have an important clinical value in improving patient management and treatment decision.

CONCLUSIONS

Our study showed that coronary ^{18}F -NaF uptake was significantly associated with the aortic ^{18}F -NaF uptake, which might imply a systematic vascular osteogenesis activation in the coronary artery and the aorta in patients with multivessel CAD. The coronary ^{18}F -NaF uptake was also correlated with the PCAT density and the coronary artery calcium score. Clinical research to validate that such a pro-atherosclerosis axis translates into a better outcome is warranted.

Acknowledgements

We are extremely grateful to Dr. Wei Yu and Dr. Lei Xu, Department of Radiology, Beijing Anzhen Hospital, Capital

Medical University Beijing, for her advice on improving the manuscript.

Disclosures

The authors have no relevant conflicts of interest to declare.

References

1. Libby P, Pasterkamp G, Crea F, Jang IK. Reassessing the mechanisms of acute coronary syndromes. *Circ Res* 2019;124:150-60.
2. Ferraro RA, van Rosendaal AR, Lu Y, Andreini D, Al-Mallah MH, Cademartiri F. Non-obstructive high-risk plaques increase the risk of future culprit lesions comparable to obstructive plaques without high-risk features: The ICONIC study. *Eur Heart J Cardiovasc Imaging* 2020;21:973-80.
3. Radcliff K, Tang TB, Lim J, Zhang Z, Abedin M, Demer LL, et al. Insulin-like growth factor-I regulates proliferation and osteoblastic differentiation of calcifying vascular cells via extracellular signal-regulated protein kinase and phosphatidylinositol 3-kinase pathways. *Circ Res* 2005;96:398-400.
4. Irlke A, Vesey AT, Lewis DY, Skepper JN, Bird JL, Dweck MR, et al. Identifying active vascular microcalcification by ¹⁸F-sodium fluoride positron emission tomography. *Nat Commun* 2015;6:7495.
5. Hoshino T, Sissani L, Labreuche J, Ducrocq G, Lavalley PC, Meseguer E, et al. Prevalence of systemic atherosclerosis burdens and overlapping stroke etiologies and their associations with long-term vascular prognosis in stroke with intracranial atherosclerotic disease. *JAMA Neurol* 2018;75:203-11.
6. Højlund-Carlsen PF, Sturek M, Alavi A, Gerke O. Atherosclerosis imaging with ¹⁸F-sodium fluoride PET: State-of-the-art review. *Eur J Nucl Med Mol Imaging* 2020;47:1538-51.
7. Li L, Li X, Jia Y, Fan J, Wang H, Fan C, et al. Sodium-fluoride PET-CT for the non-invasive evaluation of coronary plaques in symptomatic patients with coronary artery disease: A cross-correlation study with intravascular ultrasound. *Eur J Nucl Med Mol Imaging* 2018;45:2181-9.
8. Fletcher AJ, Lembo M, Kwiecinski J, Syed MBI, Nash J, Tzolos E, et al. Quantifying microcalcification activity in the thoracic aorta. *J Nucl Cardiol* 2021. <https://doi.org/10.1007/s12350-020-02458-w>.
9. Kitagawa T, Yamamoto H, Nakamoto Y, Sasaki K, Toshimitsu S, Tatsugami F, et al. Predictive Value of ¹⁸F-Sodium Fluoride Positron Emission Tomography in Detecting High-Risk Coronary Artery Disease in Combination With Computed Tomography. *J Am Heart Assoc* 2018;7:e010224.
10. Kwiecinski J, Tzolos E, Meah M, Cadet S, Adamson PD, Grodecki K, et al. Machine-learning with ¹⁸F-sodium fluoride PET and quantitative plaque analysis on CT angiography for the future risk of myocardial infarction. *J Nucl Med* 2021;63:158.
11. Bettencourt N, Toshcke AM, Leite D, Rocha J, Carvalho M, Sampaio F, et al. Epicardial adipose tissue is an independent predictor of coronary atherosclerotic burden. *Int J Cardiol* 2012;158:26-32.
12. Yamashita K, Yamamoto MH, Igawa W, Ono M, Kido T, Ebara S, et al. Association of epicardial adipose tissue volume and total coronary plaque burden in patients with coronary artery disease. *Int Heart J* 2018;59:1219-26.
13. Kitagawa T, Nakamoto Y, Fujii Y, Sasaki K, Tatsugami F, Awai K, et al. Relationship between coronary arterial ¹⁸F-sodium fluoride uptake and epicardial adipose tissue analyzed using computed tomography. *Eur J Nucl Med Mol Imaging* 2020;47:1746-56.
14. Kwiecinski J, Dey D, Cadet S, Lee SE, Otaki Y, Huynh PT, et al. Peri-coronary adipose tissue density is associated with ¹⁸F-sodium fluoride coronary uptake in stable patients with high-risk plaques. *JACC Cardiovasc Imaging* 2019;12:2000-10.
15. Kwiecinski J, Berman DS, Lee SE, Dey D, Cadet S, Lassen ML, et al. Three-hour delayed imaging improves assessment of coronary ¹⁸F-sodium fluoride PET. *J Nucl Med* 2019;60:530-5.
16. Kwiecinski J, Cadet S, Daghm M, Lassen ML, Dey D, Dweck MR, et al. Whole-vessel coronary ¹⁸F-sodium fluoride PET for assessment of the global coronary microcalcification burden. *Eur J Nucl Med Mol Imaging* 2020;47:1736-45.
17. Commandeur F, Goeller M, Betancur J, Cadet S, Doris M, Chen X, et al. Deep learning for quantification of epicardial and thoracic adipose tissue from non-contrast CT. *IEEE Trans Med Imaging* 2018;37:1835-46.
18. Scheidt M, Wesolowski M, Salazar D, Garbis N. A 3-dimensional comparison of hand and power reamers in accuracy of glenoid retroversion correction. *J Shoulder Elbow Surg* 2020;29:609-16.
19. Antonopoulos AS, Sanna F, Sabharwal N, Thomas S, Oikonomou EK, Herdman L, et al. Detecting human coronary inflammation by imaging perivascular fat. *Sci Transl Med* 2017. <https://doi.org/10.1126/scitranslmed.aal2658>.
20. Nakahara T, Strauss HW. From inflammation to calcification in atherosclerosis. *Eur J Nucl Med Mol Imaging* 2017;44:858-60.
21. Hutcheson JD, Maldonado N, Aikawa E. Small entities with large impact: microcalcifications and atherosclerotic plaque vulnerability. *Curr Opin Lipidol* 2014;25:327-32.
22. Bentzon JF, Otsuka F, Virmani R, Falk E. Mechanisms of plaque formation and rupture. *Circ Res* 2014;114:1852-66.
23. Calais F, Eriksson Ostman M, Hedberg P, Rosenblad A, Leppert J, Frobert O. Incremental prognostic value of coronary and systemic atherosclerosis after myocardial infarction. *Int J Cardiol* 2018;261:6-11.
24. Gallino A, Abovans V, Diehm C, Cosentino F, Stricker H, Falk E, et al. Non-coronary atherosclerosis. *Eur Heart J* 2014;35:1112-9.
25. Kwiecinski J, Tzolos E, Adamson PD, Cadet S, Moss AJ, Joshi N, et al. Coronary ¹⁸F-sodium fluoride uptake predicts outcomes in patients with coronary artery disease. *J Am Coll Cardiol* 2020;75:3061-74.
26. McGill HC Jr, McMahan CA, Zieske AW, Sloop GD, Walcott JV, Troxclair DA, et al. Associations of coronary heart disease risk factors with the intermediate lesion of atherosclerosis in youth. The Pathobiological Determinants of Atherosclerosis in Youth (PDAY) Research Group. *Arterioscler Thromb Vasc Biol* 2000;20:1998-2004.
27. Komatsu S, Yutani C, Ohara T, Takahashi S, Takewa M, Hirayama A, et al. Angioscopic evaluation of spontaneously ruptured aortic plaques. *J Am Coll Cardiol* 2018;71:2893-902.
28. Mazurek T, Zhang L, Zalewski A, Mannion JD, Diehl JT, Arafat H, et al. Human epicardial adipose tissue is a source of inflammatory mediators. *Circulation* 2003;108:2460-6.
29. Margaritis M, Antonopoulos AS, Digby J, Lee R, Reilly S, Coutinho P, et al. Interactions between vascular wall and perivascular adipose tissue reveal novel roles for adiponectin in the regulation of endothelial nitric oxide synthase function in human vessels. *Circulation* 2013;127:2209-21.
30. Ng AC, Goo SY, Roche N, van der Geest RJ, Wang WY. Epicardial adipose tissue volume and left ventricular myocardial function using 3-dimensional speckle tracking echocardiography. *Can J Cardiol* 2016;32:1485-92.

31. Mancio J, Barros AS, Conceicao G, Pessoa-Amorim G, Santa C, Bartosch C, et al. Epicardial adipose tissue volume and annexin A2/fetuin-A signalling are linked to coronary calcification in advanced coronary artery disease: Computed tomography and proteomic biomarkers from the EPICHEART study. *Atherosclerosis* 2020;292:75-83.
32. Tzolos E, Dweck MR. ¹⁸F-NaF for imaging microcalcification activity in the cardiovascular system. *Arterioscler Thromb Vasc Biol* 2020;2020:Atvbaha120313785.
33. Doris MK, Meah MN, Moss AJ, Andrews JPM, Bing R, Gillen R, et al. Coronary ¹⁸F-fluoride uptake and progression of coronary artery calcification. *Circ Cardiovasc Imaging* 2020;13:e011438.
34. Ishiwata Y, Kaneta T, Nawata S, Hino-Shishikura A, Yoshida K, Inoue T. Quantification of temporal changes in calcium score in active atherosclerotic plaque in major vessels by ¹⁸F-sodium fluoride PET/CT. *Eur J Nucl Med Mol Imaging* 2017;44:1529-37.
35. Roffi M, Patrono C, Collet JP, Mueller C, Valgimigli M, Andreotti F, et al. 2015 ESC Guidelines for the management of acute coronary syndromes in patients presenting without persistent ST-segment elevation: Task Force for the Management of Acute Coronary Syndromes in Patients Presenting without Persistent ST-Segment Elevation of the European Society of Cardiology (ESC). *Eur Heart J* 2016;37:267-315.
36. Joshi NV, Vesey AT, Williams MC, Shah AS, Calvert PA, Craighead FH, et al. ¹⁸F-fluoride positron emission tomography for identification of ruptured and high-risk coronary atherosclerotic plaques: a prospective clinical trial. *Lancet* 2014;383:705-13.

Publisher's Note Springer Nature remains neutral with regard to jurisdictional claims in published maps and institutional affiliations.